Q-factor optimization in dielectric oligomers

Evgeny N. Bulgakov[1,2] and Dmitrii N. Maksimov[1,2,3]
[1]*Reshetnev Siberian State University of Science and Technology, 660037 Krasnoyarsk, Russia*
[2]*Kirensky Institute of Physics, Federal Research Center KSC SB RAS, 660036 Krasnoyarsk, Russia*
[3]*Siberian Federal University, Krasnoyarsk 660041, Russia*

(Received 14 June 2019; revised manuscript received 16 August 2019; published 24 September 2019)

In this paper we propose an optimization procedure for quality-factor (Q-factor) enhancement in dielectric oligomers. The oligomers are introduced as linear periodic chains of dielectric elements the individual Q factors of which are optimized via multipolar conversion in an avoided crossing of two resonant eigenfrequencies. It is demonstrated that when such dielectric elements are assembled into an infinite periodic array the coupling between individual resonances gives rise to an in-Γ optical bound state in the continuum (BIC) unprotected by symmetry. By setting up the oligomers of finite numbers of dielectric elements we observe high quality resonances which occur as traces of the infinite array band structure. The resulting high quality resonances exhibit light localization spots of a few squared wavelengths with Q factors $Q > 10^4$. The localization is provided by similarity of the field pattern to that of the BIC with the losses at the edges of the array suppressed due to an almost flat BIC host band. The scaling law of the Q factor against the dielectric permittivity is derived.

DOI: 10.1103/PhysRevA.100.033830

I. INTRODUCTION

Controlling the localization of electromagnetic waves plays an important role in modern science and technology [1–4]. In the optical range the mainstream idea is the use of high quality (high-Q) resonant modes. This idea can be implemented with either defect modes of a two-dimensional photonic crystal [5,6] or whispering gallery modes [7,8]. Both approaches in principle allow one to engineer resonances of arbitrary high quality factors (Q factors), but at the cost of the size of the supporting structure, which in both cases is much larger than the wavelength in at least two spatial dimensions. In contrast, the application of plasmonic nanostructures easily allows for subwavelength localization [9,10], but is limited by material losses. The material losses are negligible in dielectric setups, which motivates research on near subwavelength localization of light in the field of all-dielectric nanophotonics [11,12]. The Q factor of a resonant mode supported by a single dielectric object can be significantly enhanced [13–15] if the outgoing radiation is suppressed via coupling of two radiating modes first proposed by Friedrich and Wintgen [16]. However, this approach can only lead to $Q \approx 200$ in the optical range [14] in a subwavelength dielectric system.

Another strategy to enhance the Q factor in dielectric setups is the use of bound states in the continuum (BICs) [17–19], i.e., optical nonradiating modes embedded in the continuous spectrum of the scattering states [4,20]. The major problem of that strategy is that the extremely high Q factors come at the price of the size of the resonator as the true BICs can only be hosted by dielectric structure infinitely extended at least in one spatial dimension [21]. The way around this is to employ an oligomer (finite array) of dielectric particles that preserves geometric properties of the infinitely extended photonic crystal supporting the BICs. The oligomers are formed as an infinite array is terminated at two edged points (cells). Such oligomers are known to exhibit traces of photonic band structure [22] emerging in the form of structural resonances, i.e., resonances the properties of which are dictated by spatial distribution of dielectric particles. The structural resonances may possess Q factors significantly higher than those of individual dielectric particles [23–27].

It has been recently demonstrated that the traces of BICs emerge in finite arrays of dielectric particles as high-Q structural resonances [28–30] the Q factors of which diverge algebraically with the number of particles. Engineering quasi-BIC high-Q resonances with a few elementary cells has been proposed by Taghizadeh and Chung [31]. It has been found that the structural resonances inherit the radiation pattern of traveling-wave BICs, also known as Bloch BICs [32], with radiation suppressed in the direction perpendicular to the axis of the array. Simultaneously, the radiation losses at the edges are minimized by setting up a BIC host band with flat dispersion to hinder resupply of electromagnetic energy to the lossy spots at the edges.

In this paper we propose an optimization procedure which leads to a drastic enhancement of Q factors in dielectric oligomers. Specifically, we consider parallel dielectric bars of rectangular cross section. The key idea is to employ the two mode interference mechanism by changing the cross-section aspect ratio [14] of the bar for increasing its Q factor. In this approach the Q-factor enhancement is accompanied by a dramatic change of multipolar composition of the electromagnetic field [15,33,34] with outgoing radiation suppressed in all directions, even at the level of the individual building blocks of the dielectric oligomer. We shall show that the same mechanism is responsible for formation of an in-Γ BIC unprotected by symmetry [35] in infinite arrays composed of the dielectric bars with the same geometry and permittivity. At the same time, due to weak optical coupling between the bars via outgoing radiation, the leaky band hosting the in-Γ

BIC unprotected by symmetry acquires flat dispersion which is crucial to suppress the radiation outgoing from the edges of a finite array [31]. Moreover, we shall demonstrate that the Q factor can be further optimized by varying the period of the lattice as the bar aspect ratio remains constant and deriving the scaling law of the Q factor against the dielectric permittivity.

II. OPTIMIZING THE Q FACTOR IN A SINGLE DIELECTRIC BAR

Let us consider a dielectric bar of infinite length and rectangular cross section with permittivity ϵ submersed in air. In what follows we always assume that the centerline of the bar is aligned with the z axis while the spatial extensions along the x and y axes are designated by g and h, respectively. The bar cross section in the $x0y$ plane is sketched in the inset in Fig. 1(a). Notice that in the above setting we are left with a single geometric parameter, namely, the bar cross-section aspect ratio h/g. In this paper we restrict ourselves to TM waves with zero propagation constant in the z direction. In the above stetting the electromagnetic field is exhaustively described by a single scalar variable E_z, i.e., the component of the electric vector aligned with the z axis.

By applying the Fourier modal method [36] we computed the leaky modes of a single dielectric rod in the vicinity of an avoided crossing of two resonances. The complex eigenfrequencies as a function of h/g as well as the mode profiles are shown in Fig. 1. In Fig. 1 one can see a typical picture of two branches "swapping" their field patterns in transition across the point of the avoided crossing. Notice that the eigenfields are defined up to an arbitrary normalization constant. Therefore in what follows the electric fields are measured in procedure defined units (p.d.u.) with the absolute value of the maximal field amplitude equal to the unit. As it is easily seen from Fig. 1(b) the maximal Q factor is obtained in the point marked by E in Fig. 1(b) with $h/g = 1.2914$. Remarkably, our simulations show that the position of the maximum is almost independent of ϵ. Thus, by keeping h/g constant we can recover the dependence of the Q factor on ϵ. The results are shown in Fig. 2(a). Our simulations show that with the increase of ϵ the Q factor somewhat deviates from $Q \sim \epsilon^3$, which was previously found for a single dielectric cylinder of finite length [14] with a similar field structure of the high-Q resonant mode.

It has been recently demonstrated that the maximal Q factors can be achieved due to the multipolar conversion [15], i.e., the rapid changes of multipolar structure of the rectangular wire Mie resonances [37] that suppress the far-field radiation. The multipolar expansion of the electric field outside the bar is written as

$$E_z = \sum_{m=-\infty}^{m=+\infty} a_m \frac{e^{im\phi}}{\sqrt{2\pi}} H_m^{(1)}(k_0 r), \tag{1}$$

where ϕ and r are the polar coordinates in the $x0y$ plane, k_0 is the vacuum wave number, $H_m^{(1)}$ is Hankel's function, and a_m can be found from the following formula [33]:

$$a_m = \frac{i\pi k_0^2}{2} \int_S J_m(k_0 r) \frac{e^{-im\phi}}{\sqrt{2\pi}} (\epsilon - 1) E_z(r) dr d\phi, \tag{2}$$

where J_m is the Bessel function of the first kind and the integration is performed over the bar cross section S. In Figs. 2(b) and 2(c) we plot the dominating coefficients in the multipolar expansion Eq. (1), which in our case are $m = \pm 1$ and ± 3. One can see from Fig. 2(b) that the maximal Q factor is

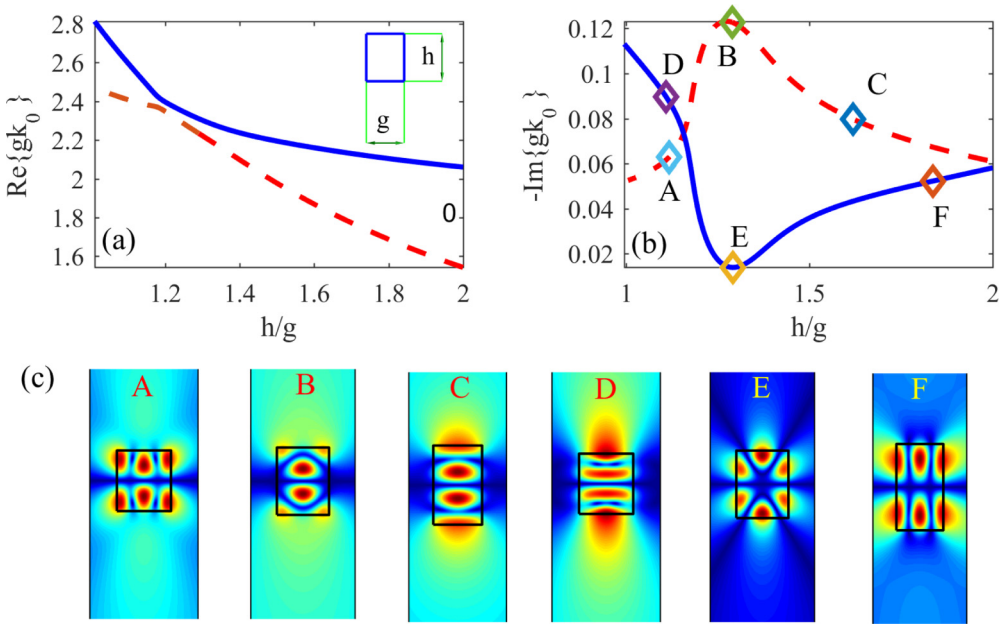

FIG. 1. The spectrum and the modes profiles in the vicinity of an avoided crossing; $\epsilon = 3.48^2$. (a) The real part of the two eigenfrequencies: high-Q resonance, solid blue line; low-Q resonance, dashed red line. (b) The imaginary parts of the two eigenfrequencies. (c) The mode profiles are shown in the bottom in the form of the absolute value of the field amplitude, $|E_z|$ (procedure defined units). The hotter spots correspond to the higher amplitude. The orientation of the structure corresponds to the inset in subplot (a). The labels attached to the mode profiles are defined in subplot (b).

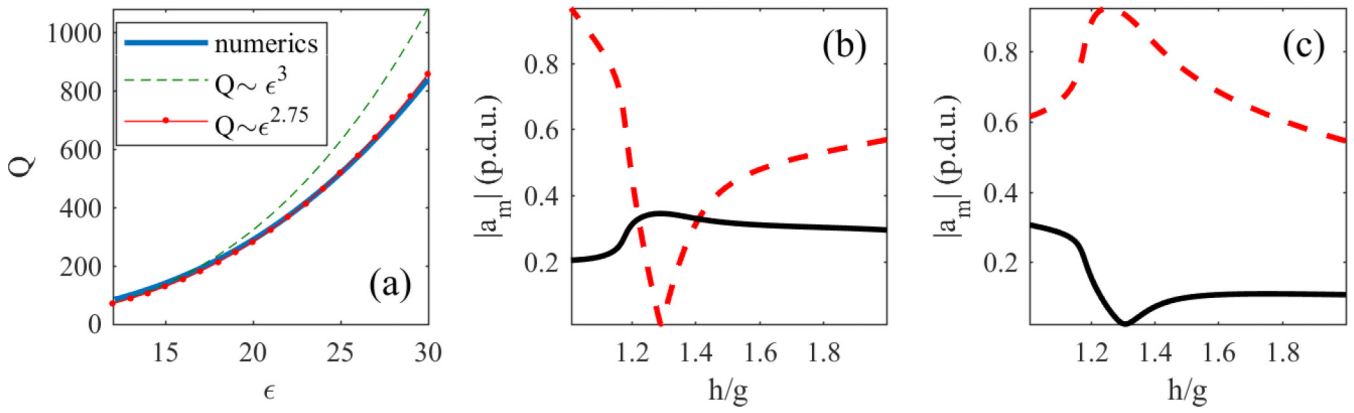

FIG. 2. Q factor and multipolar expansion of the leaky modes. (a) Maximal Q factor against ϵ, $h/g = 1.2914$. (b) Dominating expansion coefficients for the high-Q mode: $m = \pm 1$, dashed red line; $m = \pm 3$, solid black line; $\epsilon = 3.48^2$. The thin vertical line corresponds to $h/g = 1.2914$ with the maximal Q factor. (c) Dominating expansion coefficients for the low-Q mode, $\epsilon = 3.48^2$.

accompanied with a rapid change of the multipolar structure of the far-field radiation.

Following [33] we express the Q factor through the radiation rates P_m of the multipoles:

$$Q = \frac{k_0 U}{\sum P_m}, \tag{3}$$

where U is the mode energy. The radiation rate is expressed via the multipolar expansion coefficient a_m [Eq. (2)] as follows [33]:

$$P_m = \frac{1}{\pi k_0}|a_m|^2. \tag{4}$$

As it is seen from Fig. 2(b) the multipoles with $|m| = 3$ dominate in the expansion at the maximal Q factor. Therefore we truncate the summation in the denominator in Eq. (3), taking into account only the terms with $|m| = 3$. For a subwavelength solution inside the bar we can write

$$J_m(k_0 r) \sim \left(\frac{\tilde{k}_0}{\sqrt{\epsilon}} r\right)^m, \tag{5}$$

where $\tilde{k}_0 = \sqrt{\epsilon} k_0$. Using Eq. (5) one can rewrite Eq. (2) as

$$a_m \sim \frac{i\pi \tilde{k}_0^2}{2\epsilon}(\epsilon - 1)\left(\frac{\tilde{k}_0}{\sqrt{\epsilon}}\right)^m \int_S r^m \frac{e^{-im\phi}}{\sqrt{2\pi}} E_z dr d\phi. \tag{6}$$

Our simulations show that under variation of ϵ the mode shape remains unchanged, providing the same field pattern for the highest quality resonance. Thus, the integral in the above expression is independent of ϵ. Substituting Eq. (2) into Eqs. (3) and (4) and keeping in mind that $U \sim \epsilon$ one finds

$$Q \sim \frac{\epsilon^m}{\tilde{k}_0^{2(m+1)}}. \tag{7}$$

As it was already mentioned, in our case the dominant contribution is provided by the multipole with $|m| = 3$ [see Fig. 2(b)]. The quantity $\tilde{k}_0$ is almost independent of ϵ due to the persistent field structure within the bar. $\tilde{k}_0$ is, however, raised to the eighth power in the denominator in Eq. (7). Therefore, the scaling low deviates from $Q \sim \epsilon^3$. Our simulations show that in the avoided crossing regime the scaling law is best approximated by $Q \sim \epsilon^{2.75}$ as it seen from Fig. 2(b).

III. OPTIMIZING THE Q FACTOR IN AN INFINITE ARRAY OF DIELECTRIC BARS

Now we consider the system of an infinite number of coaxial dielectric bars arranged along the x axis with period a as shown in Fig. 3(a). Then, the system becomes a one-dimensional photonic crystal the spectrum of which above the line of light is a set of leaky bands. In this section we examine the leaky band of the infinite array in the spectral vicinity of the high-Q resonance obtained in the previous section with the use of the same numerical technique [36]. By using the aspect ratio h/g in Fig. 3(a) as a control parameter and keeping $a/g = 2$ we obtained the spectrum of the leaky band in the vicinity of the Γ point. Our simulations show that for the band spectrally close to the resonances in Fig. 1 a BIC emerges as the imaginary part of the in-Γ eigenfrequency vanishes at $h/g = 1.3666$, which is quite close to the highest-Q aspect ratio $h/g = 1.2914$ for a single dielectric bar.

The dispersion of this band is shown in Fig. 3(b). One can see that the imaginary part of the eigenfrequency vanishes in the Γ point as k_x^4 as it was demonstrated in [28,38]. At the same time the real part of the BIC host band has almost flat dispersion which, as it was mentioned in the introduction, is a key for designing high-Q resonances [31]. Remarkably, our simulations demonstrate that tuning h/g to obtain the BICs provides the most flat dispersive band in our setup. If h/g is detuned from the BIC point the band exhibits a more pronounced dispersion as it is seen from Fig. 3(b). In Figs. 3(c) and 3(d) we show the evolution of the in-Γ eigenfrequencies in the spectral vicinity of the Γ point. Notice that the two eigenfrequencies exhibit essentially the same behavior as those of a single dielectric bar in Figs. 1(a) and 1(b). The only difference is that in the present case the imaginary part can reach an exact zero indicating a true BIC. Finally, the mode profiles for three different aspect ratios h/g are shown in Fig. 3(e). Notice the striking resemblance between mode B in Fig. 3 and mode E in Fig. 1. Thus, as an intermediary conclusion we can state that in both cases the emergence of high-Q modes is granted by the same Friedrich-Wintgen interference mechanism [16] with the same multipoles providing the dominating contribution to expansion [Eq. (1)].

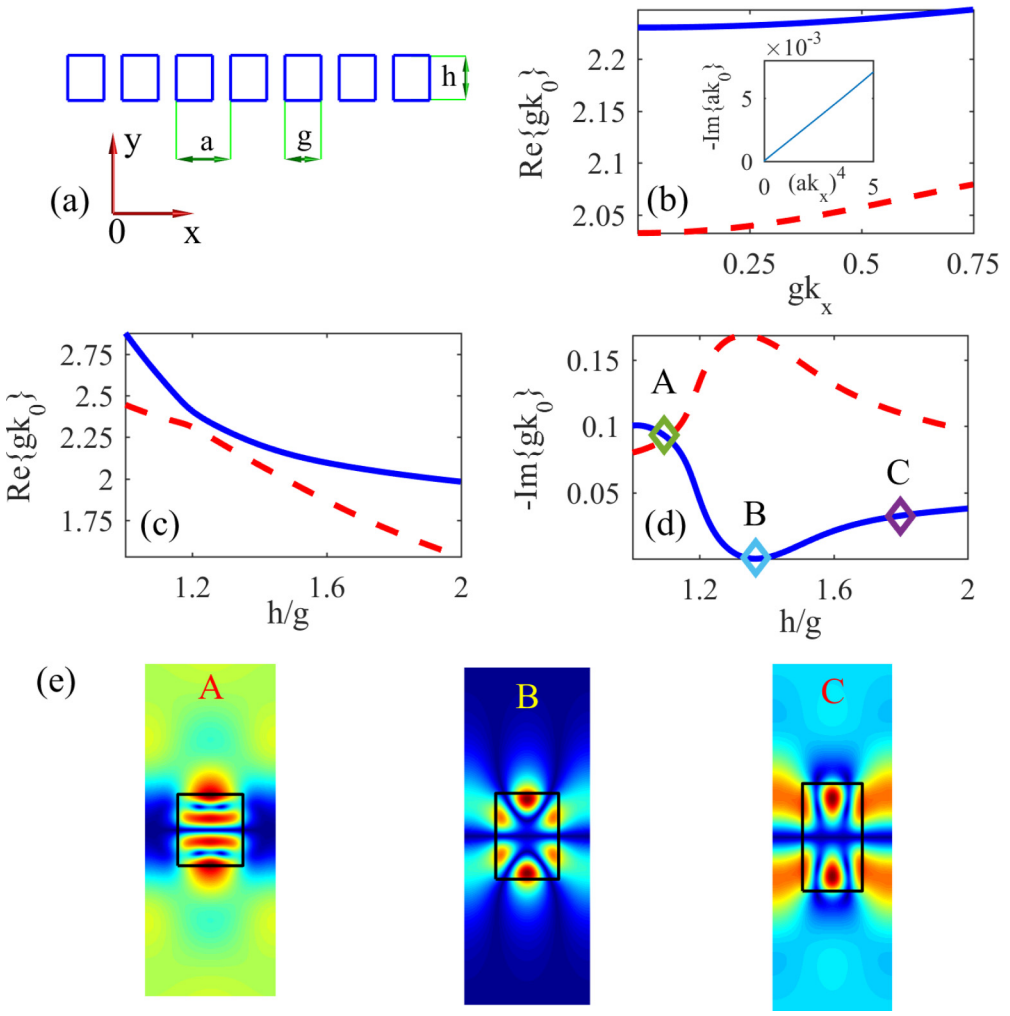

FIG. 3. Bound state in the continuum in an infinite array of dielectric bars, $a/g = 2$, $\epsilon = 3.48^2$. (a) The sketch of the system. (b) The leaky bands supported by the infinite array. Solid blue line, the real part of the eigenfrequency of the BIC host band, $h/g = 1.3666$; dashed red line, the same band at $h/g = 1.8$ with no BIC. The inset shows the dispersion of the imaginary part of the eigenfrequency of the BIC host band against k_x^4. (c) Real parts of the in-Γ eigenfrequencies against h/g. (d) Same as subplot (c) but for the imaginary part. (e) Mode profiles for high-Q resonance in subplots (c) and (d) within a single elementary cell in the form of the absolute value of the field amplitude, $|E_z|$ (p.d.u.): mode A, $h/g = 1.0955$; mode B, $h/g = 1.3666$; mode C, $h/g = 1.7990$. The orientation of the structure corresponds to the inset in subplot (a).

The field pattern of mode B in Fig. 3 is clearly symmetric with respect to $x \to x$, the same as the outgoing waves in the zeroth-order diffraction continuum at the normal incidence. This indicates an in-Γ BIC unprotected by symmetry against decay into the zeroth-order diffraction channel. We mention in passing that unlike the common symmetry protected in-Γ BICs the unprotected ones are much more difficult to set up [35] as they require a careful tuning of at least one of the parameters, h/g in our case.

IV. OPTIMIZING THE Q FACTOR IN A FINITE ARRAY OF DIELECTRIC BARS

Now assume that the infinite array is terminated at both ends to form a finite chain of N dielectric rods. In this situation we expect that the BIC unprotected by symmetry gives rise to a family of high-Q structural resonances with large N asymptotic behavior $Q \sim N^3$, as it was found in [28], and the field patterns of which within a single elementary cell are similar to those shown in Figs. 1 and 3. In Figs. 4(a)–4(c) we present the data on the Q-factor optimization procedure for an oligomer of $N = 5$ dielectric bars under variation of the aspect ratio g/h. The behavior of the high-Q eigenfrequency in Figs. 4(a) and 4(b) is similar to that in Figs. 1 and 3 while the mode profiles are drastically reshaped in transition across the point of the maximal Q factor. The simulations for $N = 5$ show that $Q = 1809$ can be achieved with the aspect ratio $g/h = 1.3580$ close to that for the BIC in the infinite array. Such Q factor exceeds the optimum for a single dielectric bar by an order of magnitude. The Q factor can be further increased by increasing the number of the bars. The mode profiles of such high-Q resonances and their Q factors are presented in Figs. 4(d) and 4(e). Notice that the field patterns represent a standing wave locked between the edges of the array with the radiation from the edges suppressed by flat dispersion of the BIC host band.

In contrast to an array of dielectric spheres and rods of circular cross section [28] the system under scrutiny possesses

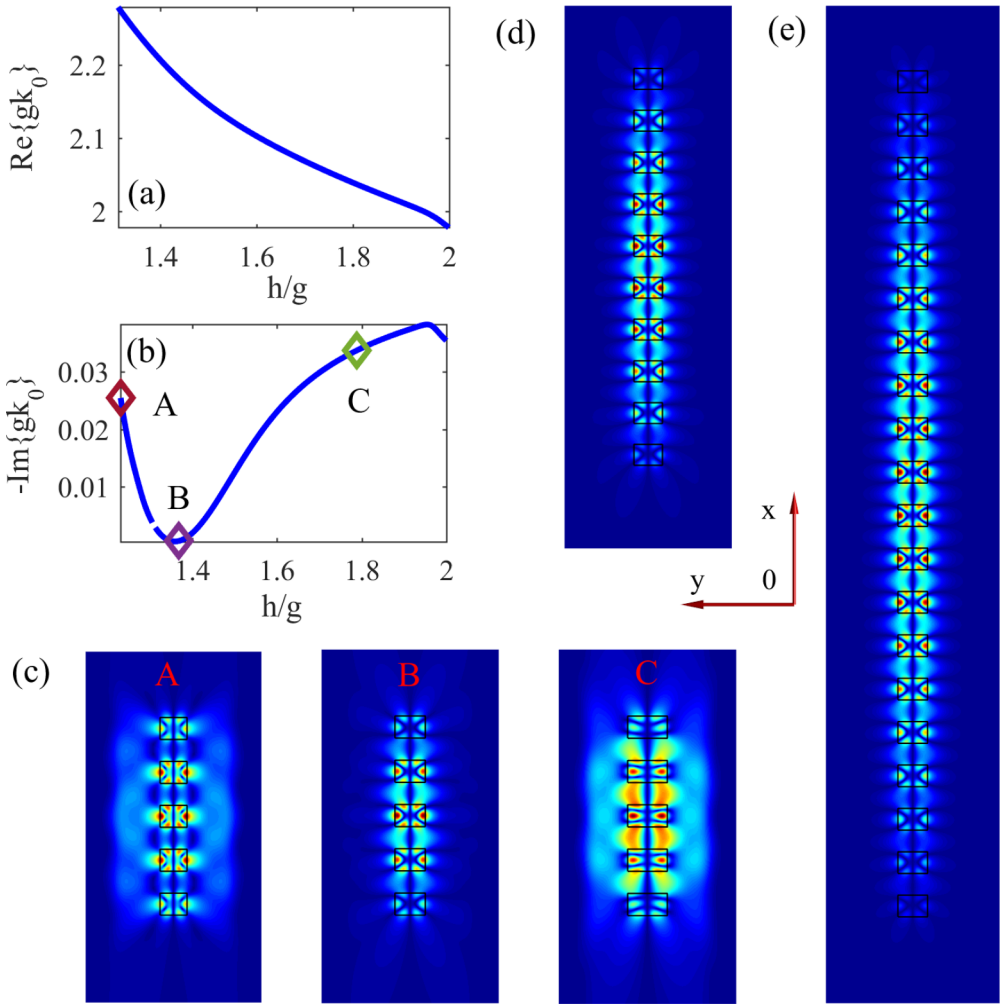

FIG. 4. High-Q resonances in oligomers of rectangular bars, $\epsilon = 3.48^2$, $a = 2g$. (a) The real part of the eigenfrequency of the high-Q resonance, $N = 5$. (b) Imaginary part of the eigenfrequency of the high-Q resonance, $N = 5$. (c) Mode profiles corresponding to the labels in subplot (b) in the form of the absolute value of the field amplitude, $|E_z|$. The highest-Q mode with $Q = 1809$, $g/h = 1.3580$ is mode B. (d) High-Q resonance, $Q = 1.18 \times 10^4$, $N = 10$, $g/h = 1.3766$. (e) High-Q resonance, $Q = 7.3 \times 10^4$, $N = 20$, $g/h = 1.3766$. The axes orientation is shown by red arrows in the middle of the plot.

one extra dimensionless geometric parameter a/g which allows for more freedom in optimizing the Q factor. Thus, the Q factor can be further increased by changing the period of the array, a. In Figs. 5(a), 5(b) and 5(e) we show the behavior of the high-Q resonances for $N = 5$ in arrays of bars with the aspect ratio $h/g = 1.3580$ found at the previous step in optimization. As before, we see the multipolar conversion similar to Figs. 1, 3, and 4. Our simulations show that with $N = 5$ the maximal Q factor, $Q = 2.85 \times 10^3$, more than twice as large as for $g = 2a$, can be achieved at $a/g = 2.1081$. In contrast to $N = 5$, for a larger number of bars, $N = 10$, the optimization with respect to $a/g = 2$ at $h/g = 1.3766$ takes no effect, resulting in the same $Q = 1.16 \times 10^4$ at $a/g = 2$, as seen from Figs. 5(c), 5(d) and 5(f). This can be qualitatively explained by similarity of the array with larger N to its infinite counterpart. It is also interesting to point out the sensitivity of the Q factor to the period of the array. One can see in Figs. 5(b) and 5(d) that the imaginary part of the eigenfrequency is rapidly increased from its minimum with the growth of the period.

Finally, let us consider excitation of high-Q resonances by a dipole source, say an atom with a two-level intra-atomic transition. The proposed setup is a key to evaluation of decay rates of a quantum system in a dielectric nanoscale environment [39]. In Fig. 6(a) we show the spectrum of the maximal amplitude of the electric-field component E_z. In Fig. 6(a) one can see pronounced peaks corresponding to the maxima of the resonant enhancement by the first two resonances induced by the BIC [28]. The field profiles at the first two maxima are shown in Figs. 6(b) and 6(c) with subplot (b) corresponding to the mode with the maximal Q factor in Fig. 4(d). Importantly, one can see that the obtained high-Q resonances can be strongly excited by a quantum two level system, the Green's function of which with the source coordinate at the position of the dipole [Figs. 6(b) and 6(c)] yields the effect of the dielectric structure onto the quantum decay rates [39].

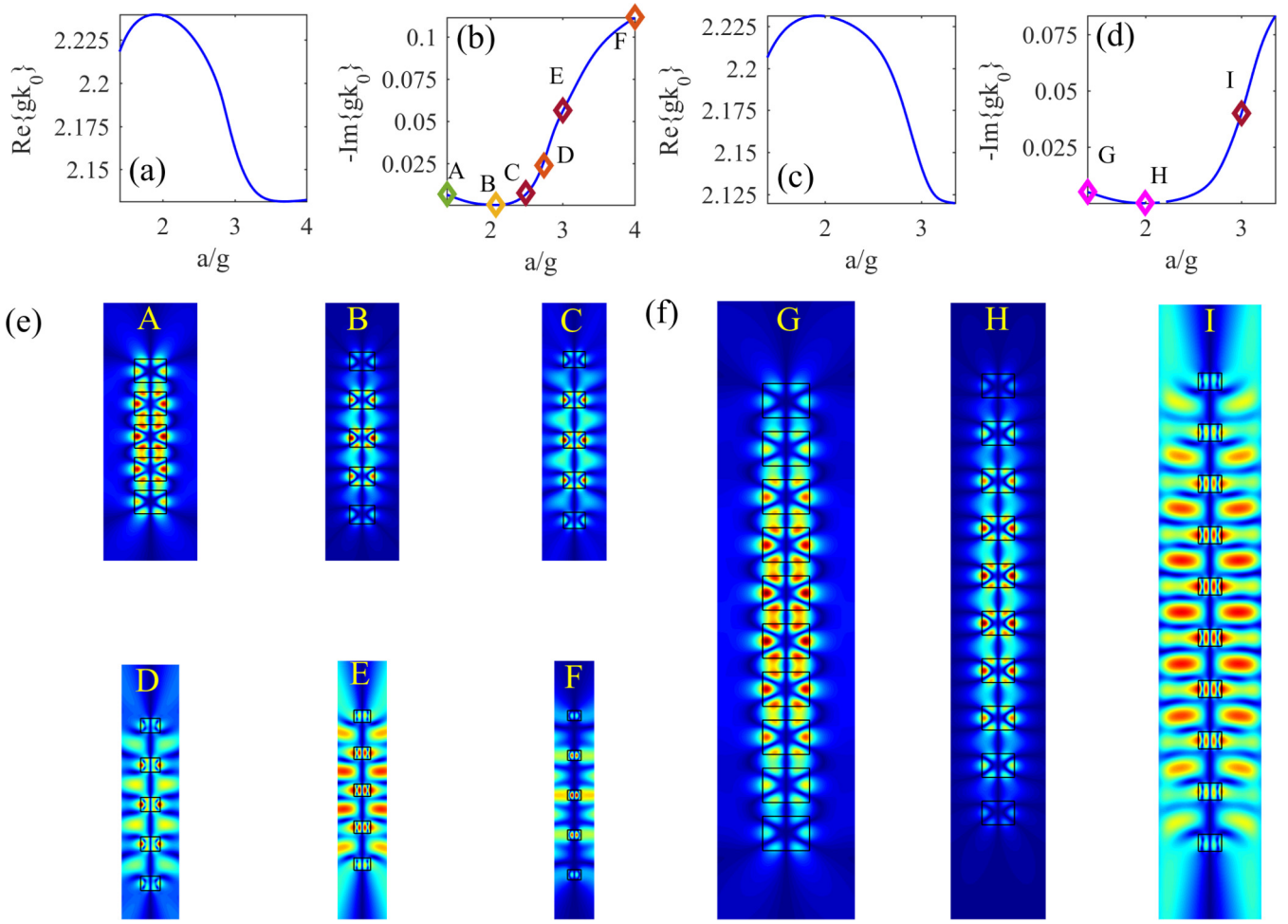

FIG. 5. Q-factor optimization by varying the period of the array, $\epsilon = 3.48^2$. (a) The real part of the eigenfrequency of the high-Q resonance, $N = 5$, $h/g = 1.3580$. (b) The imaginary part of the eigenfrequency of the high-Q resonance, $N = 5$, $h/g = 1.3580$. (c) The real part of the eigenfrequency of the high-Q resonance, $N = 10$, $h/g = 1.3766$. (d) The imaginary part of the eigenfrequency of the high-Q resonance, $N = 10$, $h/g = 1.3766$. (e) The mode profiles at resonant eigenfrequencies labeled in subplot (b) in the form of the absolute value of the field amplitude, $|E_z|$. (f) The mode profiles at resonant eigenfrequencies labeled in subplot (d). The axes orientation is the same as in Fig. 4.

V. DISCUSSION

In this paper we described a Q-factor optimization procedure in oligomers composed of a finite number of periodically arranged dielectric elements. The basic idea of the approach is increasing the number of dielectric elements limiting to an optical bound state in the continuum unprotected by symmetry. The procedure consists of four steps.

(i) The choice of the basic dielectric element which will later serve as a building block of the oligomer. In this step the geometry of the building block is optimized with respect to the maximal Q factor. The key to optimization is coupling of two resonances [13–15] accompanied by multipolar conversion [15,33,34]. In that sense the choice of rectangular bars is justified since, unlike for dielectric spheres or rods of circular cross section, the problem of resonant eigenvalues is not integrable, allowing for avoided crossing of resonances impossible in the integrable case. As a result at this step the frequency of the high-Q resonance is obtained for the optimal geometry by solving the eigenvalue problem for Maxwell's equations.

(ii) In the second step the building blocks are assembled into an infinite periodic array with period approximately twice as large as the spatial extension of the building block along the axis of periodicity. The simulations for the eigenvalues are rerun to find the optimal aspect ratio corresponding to diverging Q factor, i.e., an optical BIC. The frequency obtained in the first step provides a good initial guess in search for the BICs, since the individual building blocks are optically weakly coupled as their far-field radiation is suppressed at the Q-factor optimum. If the mode profile of the high-Q resonance is symmetric in the direction perpendicular to the axis of periodicity, the second step yields an optical BIC unprotected by symmetry hosted by a leaky band with almost flat dispersion, again due to weak optical coupling between the building blocks. The initial choice of $a = 2g$ is justified by the following arguments. First, the distance between the building blocks has to be large enough to provide weak optical coupling and, thus, guarantee a flat dispersion about the Γ point. On the other hand, the period must obey the inequality

$$a\mathrm{Re}\{k_0\} < 2\pi \tag{8}$$

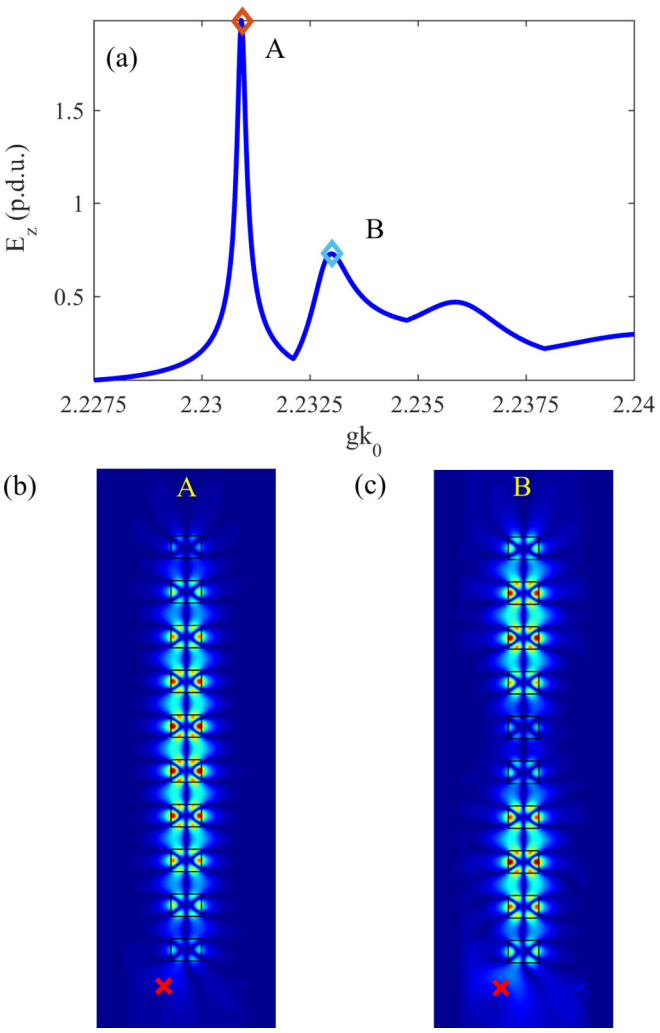

FIG. 6. Excitation of the high-Q resonances in the array with $N = 10$, $a/g = 2$, $h/g = 1.3766$, $\epsilon = 3.48^2$. (a) The spectrum of the maximal field amplitude, E_z. (b, c) The field profiles of the scattering solution at the peaks marked by A and B in subplot (a) in the form of the absolute value of the field amplitude, $|E_z|$. In subplots (b) and (c) the dipole source is located by the red cross. The axes orientation is the same as in Fig. 4.

with k_0 being the eigenfrequency found in step (i). The inequality (8) ensures the absence of the first diffraction order in the outgoing field. Otherwise, the BICs would be destroyed by leakage in the first-order diffraction channels (Wood's anomaly). In our case the data from Fig. 1 with the highest-Q resonance with $gk_0 = 2.304$ suggest that $a = 2g$ is a reasonable choice.

(iii) The infinite array is truncated to form a finite oligomer of N dielectric elements, and the optimization by changing their geometry is run again for finding the maximal Q factor. Notice that this step is much more expensive numerically, since the computational domain is N times larger than that in steps (i) and (ii). Fortunately, the frequencies of the high-Q resonance supported by the individual building block and the BIC are already known from (i) and (ii), providing the lower- and the upper-frequency bounds for high-Q resonance supported by the oligomer.

(iv) Finally, should the eigenfrequency of the high-Q resonance be different from that of the BIC, which is the case for small $N \approx 5$, a further optimization step can be taken by varying the period of the array.

In the oligomer with $N = 10$ the above procedure results in Q factors 100 times higher than in a single dielectric rod. Previously Taghizadeh and Chung [31] reported a record-high-Q quasi-BIC with $Q = 1.79 \times 10^4$ at vacuum wavelength $\lambda = 1.55\ \mu$m supported by a dielectric resonator composed of four unit cells at the same dielectric permittivity, $\epsilon = 3.48^2$. That resulted in the area of the resonator $2.2\lambda^2$ in terms of the eigenmode wavelength. In this paper we obtained $Q = 1.18 \times 10^4$ with the area of $3.2\lambda^2$ [Fig. 4(d)] and $Q = 7.3 \times 10^4$ with the area of $6.4\lambda^2$ [Fig. 4(e)]. Thus, the parameters obtained with the proposed optimization procedure provide the Q factors nearest to the best of the BIC-related setups reported in the literature [28,31] with respect to the size of the resonator. However, the primary advantage of the proposed procedure, besides its simplicity, is the scaling law against the number of dielectric elements [28], which is $Q \sim N^3$ for $N > 10$, whereas [31] reports $Q \sim N$ with saturation at $N \approx 7$.

The scaling law against permittivity, in its turn, is dictated by the multipole composition of the resonant eigenmode according to Eq. (7) and given by the index of the multipole providing the dominant contribution into the far-field radiation. We speculate that a search for resonances with higher-order multipoles could provide a faster growth of the Q factor against permittivity than $Q \sim \epsilon^3$ reported in this paper for $m = 3$. We expect that the proposed optimization procedure could be also applied to dielectric oligomers composed of three-dimensional (3D) objects. To support this claim, in the Appendix we present the numerical data on the Q-factor optimization in arrays of coaxial dielectric disks. Similarly to dielectric rods with rectangular cross section, the procedure results in $Q \approx 10^4$ at $N = 10$ and $\epsilon = 3.48^2$. Finally, the data in Fig. 6 suggest that the achieved high-Q resonances can be effectively excited by the dipole source, suggesting application to enhancement of the Purcell effect. Enhanced Purcell factors in dielectric oligomers have been previously demonstrated in [40,41]. Recently a rigorous theory of the Purcell effect with resonant eigenmodes supported by an open dielectric system was proposed in [42]. Here we restrict ourselves with a rough estimate of the Purcell factor, F, for a 3D system with a finite volume, presented in the Appendix, where we find a relatively high Purcell factor $F \approx 930$ with $N = 10$. It should be pointed out that in our estimate we neglected the material losses which would limit the Q factor in a real dielectric. We believe that enhancement of the Purcell effect by quasi-BIC is worth future study.

ACKNOWLEDGMENT

This work was supported by the Ministry of Higher Education and Science of the Russian Federation (State Contract No. 3.1845.2017/4.6).

APPENDIX: Q-FACTOR OPTIMIZATION IN A 3D SYSTEM

Here we apply the proposed optimization procedure to an oligomer composed of coaxial dielectric disks as shown in

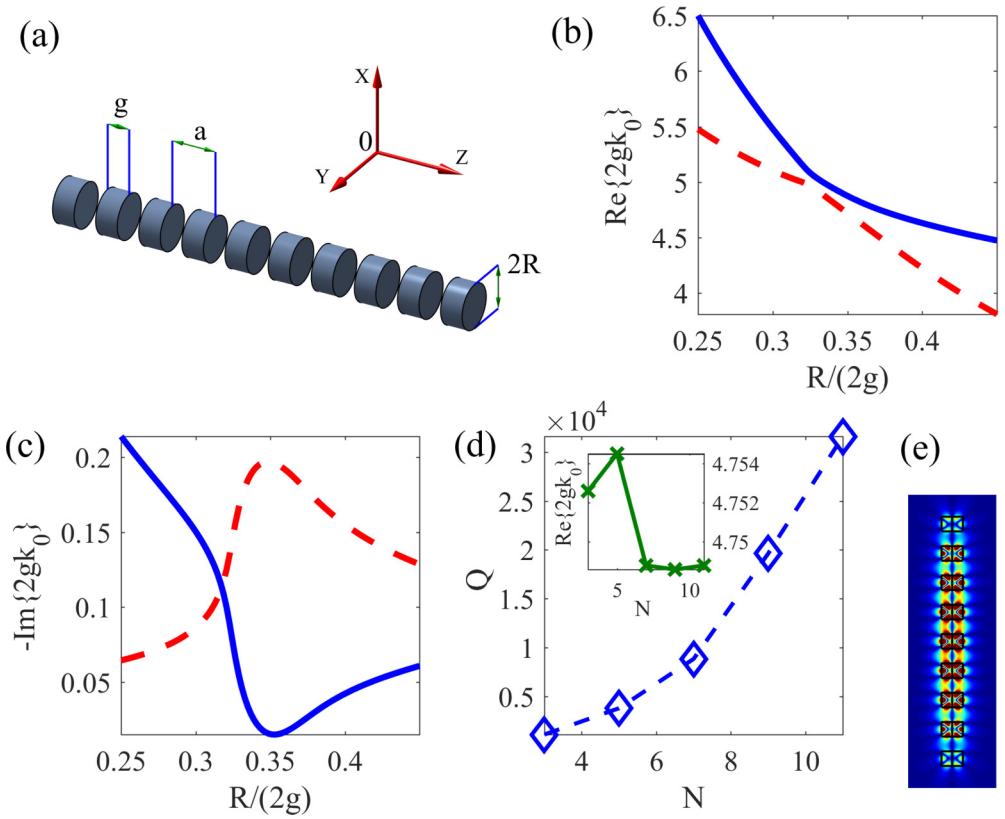

FIG. 7. (a) Oligomer composed of dielectric disks, $\epsilon = 3.48^2$ and period $a = 2g$. (b) Real parts of two resonance eigenfrequencies of a single disk in the avoided crossing regime. (c) Imaginary parts of two resonance eigenfrequencies of a single disk in the avoided crossing regime. (d) The Q factor of the structural resonances against the number of disks. The inset shows the resonant eigenfrequencies. (e) The field profile of the high-Q eigenmode with $N = 9$ and zero orbital angular momentum. The field is visualized in the form of the absolute value of the azimuthal component of the electric field, $|E_\phi|$, in the $x0z$ plane, ϕ being the azimuthal angle in the $x0y$ plane.

Fig. 7(a). To find the complex eigenfrequencies we applied the numerical method described in [43]. In the case of a single disk the problem was considered in [14] where the authors found $Q \approx 200$ with $\epsilon = 3.48^2$. This was observed due to interference of two radiating modes. The avoided crossing of the positions of the resonances is shown in Fig. 7(b), while the behavior of the imaginary parts of the resonant eigenfrequencies is demonstrated in Fig. 7(c). Notice the resemblance with Figs. 1(a) and 1(b), correspondingly. This suggests that the findings of [14] provide a good candidate for the initial step of the Q-factor optimization in the oligomer from Fig. 7(a). For optimizing the Q factor we directly applied steps (ii) and (iii) as described in Sec. V. All simulations were run for the eigenmodes with zero orbital angular momentum. At step (ii) we found that the system supports a BIC unprotected by symmetry with eigenfrequency $2gk_0 = 4.7488$ at the aspect ratio $R/(2g) = 0.36481$. At step (iii) we found that the Q factor of the BIC-related resonance supported by the oligomer is increased with the number of disks, reaching $Q \approx 2.5 \times 10^4$ with $N = 10$. Notice that this value is very close to the $N = 10$ resonance in Fig. 4(d). The dependence of the Q factor on N is shown in Fig. 7(d). The frequencies of the high-Q resonances are shown in the inset to Fig. 7(d). Finally, in Fig. 7(e) we plot the field profile of the high-Q mode with $N = 9$.

Relying on the above data we can roughly estimate the Purcell factor using the formula

$$F = \frac{6\pi Q}{\mathrm{Re}\{k_0\}^3 V} \tag{A1}$$

with V as the mode volume. Since the high-Q eigenmode is well localized in the oligomer, as it is seen from Fig. 7(e), we estimate the mode volume as the volume of the dielectric disks plus the blank spaces between them through the formula $V \approx \pi R^2 g(2N - 1)$. This rough estimation yields a relatively high Purcell factor $F \approx 930$ with $N = 10$. Notice, however, that this value is obtained for an ideal dielectric with no material losses, and neglecting the correct definition of the mode volume introduced in [42].

[1] S. John, Why trap light? Nat. Mater. **11**, 997 (2012).
[2] D. Marpaung, C. Roeloffzen, R. Heideman, A. Leinse, S. Sales, and J. Capmany, Integrated microwave photonics, Laser and Photonics Rev. **7**, 506 (2013).
[3] P. Qiao, W. Yang, and C. J. Chang-Hasnain, Recent advances in high-contrast metastructures, metasurfaces, and photonic crystals, Adv. Opt. Photonics **10**, 180 (2018).

[4] C. Wei Hsu, B. Zhen, A. Douglas Stone, J. D. Joannopoulos, and M. Soljačić, Bound states in the continuum, Nat. Rev. Mater. **1**, 16048 (2016).
[5] O. Painter, J. Vučkovič, and A. Scherer, Defect modes of a two-dimensional photonic crystal in an optically thin dielectric slab, J. Opt. Soc. Am. B **16**, 275 (1999).
[6] T. Asano, Y. Ochi, Y. Takahashi, K. Kishimoto, and S. Noda, Photonic crystal nanocavity with a Q factor exceeding eleven million, Opt. Express **25**, 1769 (2017).
[7] V. B. Braginsky, M. L. Gorodetsky, and V. S. Ilchenko, Quality-factor and nonlinear properties of optical whispering-gallery modes, Phys. Lett. A **137**, 393 (1989).
[8] M. L. Gorodetsky and V. S. Ilchenko, Optical microsphere resonators: Optimal coupling to high-Q whispering-gallery modes, J. Opt. Soc. Am. B **16**, 147 (1999).
[9] J. A. Dionne, L. A. Sweatlock, H. A. Atwater, and A. Polman, Plasmon slot waveguides: Towards chip-scale propagation with subwavelength-scale localization, Phys. Rev. B **73**, 035407 (2006).
[10] O. Hess, J. B. Pendry, S. A. Maier, R. F. Oulton, J. M. Hamm, and K. L. Tsakmakidis, Active nanoplasmonic metamaterials, Nat. Mater. **11**, 573 (2012).
[11] R. S. Savelev, S. V. Makarov, A. E. Krasnok, and P. A. Belov, From optical magnetic resonance to dielectric nanophotonics (a review), Opt. Spectrosc. **119**, 551 (2015).
[12] S. Jahani and Z. Jacob, All-dielectric metamaterials, Nat. Nanotechnology **11**, 23 (2016).
[13] J. Wiersig, Formation of Long-Lived, Scarlike Modes Near Avoided Resonance Crossings in Optical Microcavities, Phys. Rev. Lett. **97**, 253901 (2006).
[14] M. V. Rybin, K. L. Koshelev, Z. F. Sadrieva, K. B. Samusev, A. A. Bogdanov, M. F. Limonov, and Y. S. Kivshar, High-Q Supercavity Modes in Subwavelength Dielectric Resonators, Phys. Rev. Lett. **119**, 243901 (2017).
[15] W. Chen, Y. Chen, and W. Liu, Subwavelength high-Q Kerker supermodes with unidirectional radiations, arXiv:1808.05539.
[16] H. Friedrich and D. Wintgen, Interfering resonances and bound states in the continuum, Phys. Rev. A **32**, 3231 (1985).
[17] S. Romano, I. Rendina, and V. Mocella, High field enhancement factors in photonic nanostructures, in Proceedings of the 2015 AEIT International Annual Conference (unpublished) (2015).
[18] V. Mocella and S. Romano, Giant field enhancement in photonic resonant lattices, Phys. Rev. B **92**, 155117 (2015).
[19] J. W. Yoon, S. H. Song, and R. Magnusson, Critical field enhancement of asymptotic optical bound states in the continuum, Scientific Reports **5**, 18301 (2015).
[20] K. Koshelev, G. Favraud, A. Bogdanov, Y. Kivshar, and A. Fratalocchi, Nonradiating photonics with resonant dielectric nanostructures, Nanophotonics **8**, 725 (2019).
[21] M. G. Silveirinha, Trapping light in open plasmonic nanostructures, Phys. Rev. A **89**, 023813 (2014).
[22] A. Yamilov and H. Cao, Density of resonant states and a manifestation of photonic band structure in small clusters of spherical particles, Phys. Rev. B **68**, 085111 (2003).
[23] S. V. Boriskina, Theoretical prediction of a dramatic Q-factor enhancement and degeneracy removal of whispering gallery modes in symmetrical photonic molecules, Opt. Lett. **31**, 338 (2006).
[24] U. Zywietz, M. K. Schmidt, A. B. Evlyukhin, C. Reinhardt, J. Aizpurua, and B. N. Chichkov, Electromagnetic resonances of silicon nanoparticle dimers in the visible, ACS Photonics **2**, 913 (2015).
[25] A. A. Dmitriev and M. V. Rybin, Strong optical coupling combines isolated scatterers into dimer, Phys. Rev. A **99**, 063837 (2019).
[26] E. Bulgakov, K. Pichugin, and A. Sadreev, Evolution of the resonances of two parallel dielectric cylinders with distance between them, arXiv:1906.02409.
[27] K. N. Pichugin and A. F. Sadreev, Interaction between coaxial dielectric disks enhances the Q-factor, arXiv:1905.04856.
[28] E. N. Bulgakov and D. N. Maksimov, Light enhancement by quasi-bound states in the continuum in dielectric arrays, Opt. Express **25**, 14134 (2017).
[29] E. N. Bulgakov and A. F. Sadreev, High-Q resonant modes in a finite array of dielectric particles, Phys. Rev. A **99**, 033851 (2019).
[30] Z. F. Sadrieva, M. A. Belyakov, M. A. Balezin, P. V. Kapitanova, E. A. Nenasheva, A. F. Sadreev, and A. A. Bogdanov, Experimental observation of a symmetry-protected bound state in the continuum in a chain of dielectric disks, Phys. Rev. A **99**, 053804 (2019).
[31] A. Taghizadeh and I.-S. Chung, Quasi bound states in the continuum with few unit cells of photonic crystal slab, Appl. Phys. Lett. **111**, 031114 (2017).
[32] E. N. Bulgakov and A. F. Sadreev, Bloch bound states in the radiation continuum in a periodic array of dielectric rods, Phys. Rev. A **90**, 053801 (2014).
[33] S. G. Johnson, S. Fan, A. Mekis, and J. D. Joannopoulos, Multipole-cancellation mechanism for high-Q cavities in the absence of a complete photonic band gap, Appl. Phys. Lett. **78**, 3388 (2001).
[34] Q. H. Song and H. Cao, Improving Optical Confinement in Nanostructures via External Mode Coupling, Phys. Rev. Lett. **105**, 053902 (2010).
[35] E. N. Bulgakov and A. F. Sadreev, Light trapping above the light cone in a one-dimensional array of dielectric spheres, Phys. Rev. A **92**, 023816 (2015).
[36] M. Pisarenco, J. Maubach, I. Setija, and R. Mattheij, Modified S-matrix algorithm for the aperiodic fourier modal method in contrast-field formulation, J. Opt. Soc. Am. A **28**, 1364 (2011).
[37] P. E. Landreman, H. Chalabi, J. Park, and M. L. Brongersma, Fabry-Perot description for Mie resonances of rectangular dielectric nanowire optical resonators, Opt. Express **24**, 29760 (2016).
[38] L. Yuan and Y. Yan Lu, Strong resonances on periodic arrays of cylinders and optical bistability with weak incident waves, Phys. Rev. A **95**, 023834 (2017).
[39] L. Novotny and B. Hecht, *Principles of Nano-Optics* (Cambridge University, Cambridge, England, 2012).
[40] A. Krasnok, S. Glybovski, M. Petrov, S. Makarov, R. Savelev, P. Belov, C. Simovski, and Y. Kivshar, Demonstration of the

enhanced Purcell factor in all-dielectric structures, Appl. Phys. Lett. **108**, 211105 (2016).

[41] R. S. Savelev, O. N. Sergaeva, D. G. Baranov, A. E. Krasnok, and A. Alù, Dynamically reconfigurable metal-semiconductor Yagi-Uda nanoantenna, Phys. Rev. B **95**, 235409 (2017).

[42] E. A. Muljarov and W. Langbein, Exact mode volume and Purcell factor of open optical systems, Phys. Rev. B **94**, 235438 (2016).

[43] F. Bigourdan, J.-P. Hugonin, and P. Lalanne, Aperiodic-fourier modal method for analysis of body-of-revolution photonic structures, J. Opt. Soc. Am. A **31**, 1303 (2014).